Extraction of the ^{12}C Longitudinal and Transverse Nuclear Electromagnetic Response Functions from all Electron Scattering Measurements on Carbon

Arie Bodek,[1] M. E. Christy,[2] Zihao Lin,[1] and A. Ankowski[3]

[1]*Department of Physics and Astronomy, University of Rochester, Rochester, NY 14627, USA**
[2]*Thomas Jefferson National Accelerator Facility, Newport News, VA 23606, USA*†
[3]*University of Wroclaw, Wroclaw, Poland*

(Dated: March 9, 2024)

We report on a global extraction of the ^{12}C Longitudinal ($\mathcal{R}_L$) and Transverse ($\mathcal{R}_T$) nuclear electromagnetic response functions from an analysis of all available electron scattering dats on carbon. The response functions are extracted for a large range of energy transfer ν, spanning the nuclear excitation, quasielastic, resonance and inelastic continuum over a large range of the square of the four-momentum transfer Q^2. We extract $\mathcal{R}_L$ and $\mathcal{R}_T$ as a function of ν for both fixed values of Q^2 ($0 \leq Q^2 \leq 3.5$ GeV^2), as well fixed values of momentum transfer $\mathbf{q}$ $0.1 \leq \mathbf{q} \leq 3.75$ GeV). The data sample consists of about 16,000 ^{12}C differential electron scattering and photo-absorption-cross section measurements. Since the extracted response functions cover a large range of Q^2 and ν, they can be readily used to validate both nuclear models as well Monte Caro (MC) generators for electron and neutrino scattering experiments. The extracted response functions are compare to the prediction of several theoretical models and to predictions of the electron-mode versions of the NuWro and GENIE neutrino MC generators.

I. INTRODUCTION

Electron scattering cross sections on nuclear targets are completely described by Longitudinal ($\mathcal{R}_L$) and Transverse ($\mathcal{R}_T$) nuclear electromagnetic response functions for each nuclear target. Here $\mathcal{R}_T$ and $\mathcal{R}_T$ are functions of the energy transfer ν (or excitation energy E_x)) and the square of the 4-momentum transfer Q^2 (or alternatively the 3-momentum transfer $\mathbf{q}$). Recent theoretical calculations[1–5] of $\mathcal{R}_L(\mathbf{q},\nu)$ and $\mathcal{R}_T(\mathbf{q},\nu)$ can tested by comparing the predictions to experimental data. In this paper we extract both response functions as functions of $(\mathbf{q},\nu)$ as well as (Q^2,ν) from an analysis of all available cross section data for ^{12}C. Since our extracted response functions cover a large range of Q^2 and ν, they can be readily used to validate both nuclear models as well Monte Caro generators for electron and neutrino scattering experiments.

A previous extraction of $\mathcal{R}_T(\mathbf{q},\nu)$ and $\mathcal{R}_L(\mathbf{q},\nu)$ from experimental cross section data in the quasielastic (QE) region was published in Jourdan:96[8, 9] for 3 values of momentum transfer ($\mathbf{q}$=0.30, 0.38 and 0.57 GeV) over a limited range of ν. Earlier extraction in a similar kinematic region were published in Barreau:81[10] (for the square of the 4-momentum transfer Q^2=0.16 GeV^2) and in Barreau:82[11] (for $\mathbf{q}$=0.30, 0.40 and 0.55 GeV).

For a small range of nuclear excitation energies of 16$<$ E_x $<$40 MeV, values of $\mathcal{R}_L(\mathbf{q},E_x)$ and $\mathcal{R}_T(\mathbf{q},E_x)$ are reported in Yamafuchi:71 [6] for smaller values of $\mathbf{q}$ values (0.148, 0.167, 0.205, 0.240 and 0.307 GeV.)

In this communication we report on the extraction of $\mathcal{R}_L$ and $\mathcal{R}_T$ for ^{12}C from an analysis of all available electron scattering cross section measurements on carbon. As summarized in Table I, the response functions are extracted for a large range of energy transfer ν for fixed values of Q^2 ($0 < Q^2 < 3.5$ GeV^2) as well as fixed values of $\mathbf{q}$ ($0.1 < \mathbf{q} < 3.75$ GeV). The range of ν span the nuclear excitation, QE, resonance and inelastic continuum. The data sample consists of about 16,000 ^{12}C differential cross section measurements as well as photo-absorption data (Q^2=0). Because additional cross section measurements are included in our analysis, our extracted values of $\mathcal{R}_L$) and $\mathcal{R}_T$ for ^{12}C are more precise and span a larger kinematic range than previous analyses. S The extractions of $\mathcal{R}_L$ and $\mathcal{R}_T$ for ^{12}C in the higher resonance and inelastic continuum regions, as well as for other nuclei will be reported in future communications.

A. Overview of this analysis

In two previous papers[12, 13] we describe universal fits to all available cross section measurements for ^{12}C. We have also done similar fits for other nuclei. The fits describe all data in the nuclear excitation, QE, resonance, and inelastic continuum regions from the Q^2=0 photo-absorptionlimit to Q^2 values in the deep inelastic multi GeV^2 region. These fits are primarily used for the calculation of radiative corrections in electron scattering experiments.

In addition, these fits are also are essential for this analysis for the following reasons. The Rosenbluth extractions of $\mathcal{R}_T(Q^2,\nu))$ and $\mathcal{R}_L(Q^2,\nu)$ require cross sec-

*Electronic address: bodek@pas.rochester.edu
†Electronic address: christy@jlab.org

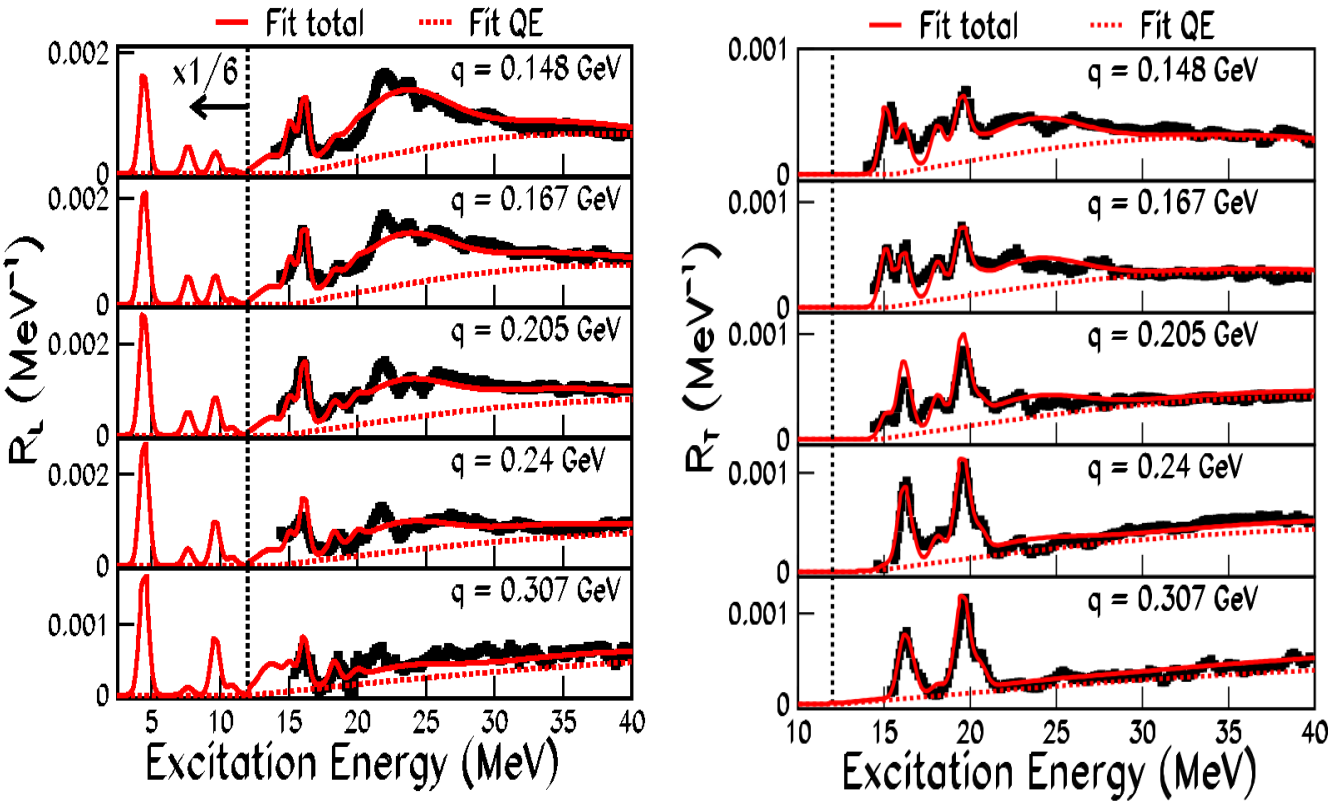

FIG. 1: Comparison of the ^{12}C longitudinal (R_L/Z^2, left) and transverse ($\mathcal{R}_T/Z^2$, right) response functions extracted by Yamaguchi:71 [6] (black squares) versus excitation energy E_x, to the response functions extracted from our universal fit to all available electron scattering cross section data on ^{12}C (solid red line). The contributions from excitation energies less than 12 MeV are multiplied by (1/6). The QE contribution to the total response functions is represented by the red dashed line. In our fit, we model the response functions for all states the region of the Giant Dipole Resonance (20-30 MeV) region as one average broad excitation. Note there are no transverse states with $E_x < 10$ MeV.

tion measurements at different angles for the same values of Q^2 and ν. In our analysis we bin the data in Q^2 (or $\mathbf{q}$) and ν bins. We use the fits for "bin centering corrections) corrections to account for the difference in Q^2 and ν of the cross sections measurements at the different angles.

In our fits, cross sections for nuclear excitations are described by fits to measurements of transverse and longitudinal form factors [13] for each nuclear state. In our overall fit these cross sections are added to the fit for the QE cross section. A comparison of ^{12}C $\mathcal{R}_L/Z^2$ and $\mathcal{R}_T/Z^2$ measurements published in Yamaguchi:71 [6] for the nuclear excitation region ($E_x < 40$ MeV) to $\mathcal{R}_L/Z^2$ and $\mathcal{R}_T/Z^2$ extracted from our overall fit is shown in Figure 1.

Rosenbluth extractions of $\mathcal{R}_L$ and $\mathcal{R}_T$ using data spanning a range of angles from different experiments is valid in the QE and pion production regions. However, in the nuclear excitation region it is not valid to combine experiments with different experimental resolutions. For example, in the left panel of Fig. 2 we show a comparison of high resolution extraction of $\mathcal{R}_T$ in Yamaguchi:71 [6] for Q^2=0.085 GeV^2 to $\mathcal{R}_T$ extracted from the lower resolution 180^0 cross section data published in Ryan:84[7]. As shown in the right panel of Fig. 2 the contribution from nuclear excitation is significant a low Q^2 (or $\mathbf{q}$). Therefore in the nuclear excitation region $16 < E_x < 40$ MeV we use the precise ($\pm$3%) Yamaguchi :71 measurements of $\mathcal{R}_L$ and $\mathcal{R}_T$. In addition, for $\mathcal{R}_T$, we also use electron scattering data at 180^0 as shown in Fig. 3.

For E_x <16 MeV we extract $\mathcal{R}_L$ and $\mathcal{R}_T$ from our overall fits [13] to the nuclear excitation form factors. (shown as the red solid line in Figure 1). For E_x >30 MeV, we extract $\mathcal{R}_L$ and $\mathcal{R}_T$ from our analysis of all available electron scattering data as described below.

X

II. INCLUSIVE ELECTRON-NUCLEON SCATTERING

In terms of the incident electron energy, E_0, the scattered electron energy, $E^{'}$, and the scattering angle, θ, the

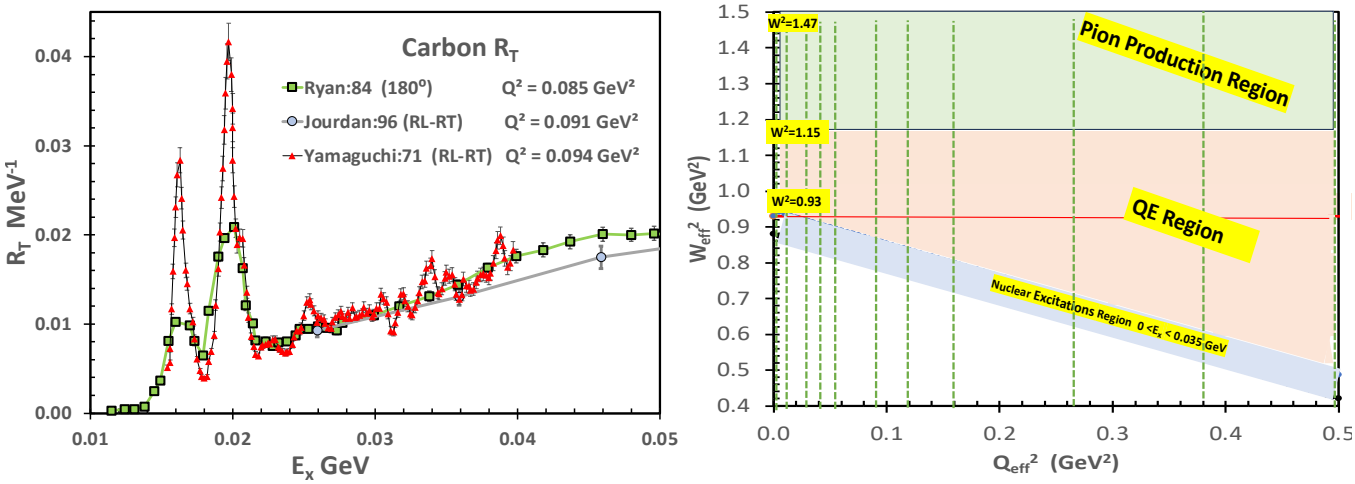

FIG. 2: Left: Comparison of the high resolution measurements of $\mathcal{R}_T$ in Yamaguchi:71 [6] for Q^2=0.085 GeV^2 (versus E_x) to values of $\mathcal{R}_T$ extracted from the lower resolution 180^0 electron scattering cross-section measurements published in Ryan:84[7] (multiplied by 1.05). Right: W^2 range for the fixed Q^2 values investigated in this analysis. At low Q^2 (or **q**) the contribution from nuclear excitation is significant.

q	Q^2 Published E_x <40 MeV	Ref	**q**	Q^2 Published E_x >20 MeV	Ref.	Center Q^2	Q^2 low	Q^2 high	Center **q**	$\mathcal{R}_T$ ν=**q**	**q** low	**q** high
	0 ($\gamma^{12}C$)	$\mathcal{R}_T$[14–18]		0($\gamma^{12}C$)	$\mathcal{R}_T$[14–18]	0	0	0		From $\gamma^{12}C$	NA	NA
0.100	0.006-0.010	$\mathcal{R}_T(180^0)$[19]										
0.100	0.013-0.015	$\mathcal{R}_T(180^0)$[20]				0.010	0.004	0.015	**0.100**	0.0016±0.0004	0.063	0.124
0.148	0.020 -0.022	$\mathcal{R}_L\mathcal{R}_L$[6]				0.020	0.015	0.025	**0.148**	0.0021±0.0007	0.124	0.158
0.167	0.026-0.027	$\mathcal{R}_L\mathcal{R}_L$[6]		.		0.026	0.025	0.035	**0.167**	0.0028±0.0006	0.158	0.186
0.205	0.040-0.042	$\mathcal{R}_L\mathcal{R}_L$[6]	0.033-0.085	$\mathcal{R}_T(180^0)$[7]		0.040	0.035	0.045	**0.205**	0.0071±0.0007	0.186	0.223
0.240	0.056-0.057	$\mathcal{R}_L\mathcal{R}_L$[6]	0.033-0.085	$\mathcal{R}_T(180^0)$[7]		0.056	0.045	0.070	**0.240**	0.0134±0.0009	0.223	0.270
0.307	0.093-0.094	$\mathcal{R}_L\mathcal{R}_L$[6]	0.070-0.089	$\mathcal{R}_L\mathcal{R}_L$[8, 9]	**0.300**	0.093	0.070	0.100	**0.300**	0.0270±0.0006	0.270	0.340
0.300	0.033-0.085	$\mathcal{R}_T(180^0)$[7]	0.058-0.090	$\mathcal{R}_L\mathcal{R}_L$[11]	**0.300**							
0.380			0.100-0.144	$\mathcal{R}_L\mathcal{R}_L$[8, 9]	**0.380**	0.120	0.100	0.145	**0.380**	0.0324±0.0005	0.340	0.428
			0.079-0.160	$\mathcal{R}_L\mathcal{R}_L$[11]	**0.400**							
0.475			0.16	$\mathcal{R}_L\mathcal{R}_L$[10]		0.160	0.145	0.209	**0.475**	0.0276±0.0005	0.428	0.523
			0.171-0.301	$\mathcal{R}_L\mathcal{R}_L$[11]	**0.550**							
0.570			0.206-0.323	$\mathcal{R}_L\mathcal{R}_L$[8, 9]	**0.570**	0.265	0.206	0.323	**0.570**	0.0262±0.0008	0.523	0.609
0.649					**0.649**	0.380	0.322	0.438	**0.649**	0.0290±0.0006	0.609	0.702
0.756					**0.756**	0.500	0.438	0.650	**0.756**	0.0299±0.0010	0.702	0.878
0.991					**0.991**	0.800	0.650	1.050	**0.991**	0.0339±0.0003	0.878	1.302
1.619					**1.619**	1.250	1.050	1.500	**1.619**	0.0420±0.0010	1.302	1.770
1.921					**1.921**	1.750	1.500	2.000	**1.921**	0.0470±0.0010	1.770	2.067
2.213					**2.213**	2.250	2.000	2.500	**2.213**	0.0545±0.0020	2.067	2.357
2.500					**2.500**	2.750	2.500	3.000	**2.500**	0.0630±0.0030	2.357	2.642
2.783					**2.783**	3.250	3.000	3.500	**2.783**	0.0700±0.0030	2.642	2.923
3.500					**3.500**	3.750	3.500	4.000	**3.500**	0.00?0±0.0030	2.923	4.500

TABLE I: A summery of the bins in Q^2 (in GeV^2) and in **q** (in GeV). Also shown are the kinematic range of previous measurements [6, 8, 9, 11]. The $\mathcal{R}_T$ experimental values for $\nu = \underline{q}$ are extracted from photo-absorption-cross sections.

absolute value of the exchanged 4-momentum squared in electron-nucleon scattering is given by

$$Q^2 = (-q)^2 = 4E_0E^{'}\sin^2\frac{\theta}{2}, \quad (1)$$

the mass of the undetected hadronic system is

$$W^2 = M^2 + 2M\nu - Q^2, \quad (2)$$

and the square of the magnitude of 3-momentum transfer vector $\vec{\mathbf{q}}$ is

$$\mathbf{q}^2 = Q^2 + \nu^2 \quad (3)$$

Here M the average nucleon mass and $\nu = E_0 - E'$. In these expressions we have neglected the electron mass which is negligible for the kinematics studied.

For scattering from a nuclear target such as carbon, the excitation energy E_x is given by $E_x = \nu - \nu_{elastic}$

	Data Set	Q^2_{Min} (GeV^2)	Q^2_{Max} (GeV^2)	# Data Points	Normalization	Error
1	Barreau83 [11]				0.99185	
2	O'Connell87 [28]				0.97869	
3	Sealock89 [29]				1.0315	
4	Baran88 [30]				0.99241	
5	Bagdasaryan88 [31]				0.98777	
6	Dai19 [32]				1.0108	
7	Arrington96[33]				0.97427	
8	Day93 [34]				1.0071	
9	Arrington99 [35]				0.98884	
10	Gaskell21 [36, 37]				0.99340	
11	Whitney74 [38, 39]				1.0149	
12	E04-001-2005 (preliminary) [40–42]				0.99812	
13	E04-001-2007 (preliminary) [40–42]				1.0029	
14	Gomez74 [43, 44]				1.0125	
15	Fomin10 [45, 46]				1.0046	
16	Yamaguchi71 [6]				1.0019	
17	Ryan84 [7]				1.0517	
18	Czyk63 [47]				1.25	0.1
19	Bounin63 [48, 49]				1.15	0.1
20	Photo-Daphne				0.99754	
21	Spamer70 [6, 50]				1.1	
22	Goldemberg64 [19]				1.1	0.1
23	Deforest65 [20]				0.85	0.1
	Donnelly68 [51, 52] (not used)					
	Zeller73 [53] (not used)					

TABLE II: A summary table of the ^{12}C data sets used in the universal fit. Shown are the number of data points, the Q^2 range of each set, the normalization factor, and the universal fit χ^2 per degree of freedom for each set. The Zeller73 [53] data set is inconsistent with all other data sets and is not used.

where

$$\nu_{elastic} = E_0 - \frac{E_0}{1 + 2E_0 \sin^2\frac{\theta}{2}/M_A}, \tag{4}$$

and M_A is the mass of the nuclear target (for carbon $M_{A=12}$=11.178 GeV). Or equivalently

$$E_x = \nu - \frac{Q^2_{elastic}}{2M_A}, \tag{5}$$

where $Q^2_{elastic}$ is Q^2 for elastic scattering from a carbon nucleus for incident energy E_0 and scattering angle θ.

A. Description in terms of longitudinal and transverse virtual photon cross sections

This description is often used in the resonance region. In the one-photon-exchange approximation, the spin-averaged cross section for inclusive electron-proton scattering can be expressed in terms of the photon helicity coupling as

$$\frac{d\sigma}{d\Omega dE'} = \Gamma\left[\sigma_T(W^2, Q^2) + \epsilon\sigma_L(W^2, Q^2)\right], \tag{6}$$

where σ_T (σ_L) is the cross section for photo-absorption of purely transverse (longitudinal) polarized photons,

$$\Gamma = \frac{\alpha E'(W^2 - M_N^2)}{(2\pi)^2 Q^2 M E_0(1-\epsilon)} \tag{7}$$

is the flux of virtual photons, $\alpha = 1/137$ is the fine structure constant, and

$$\epsilon = \left[1 + 2(1 + \frac{\nu^2}{Q^2})\tan^2\frac{\theta}{2}\right]^{-1} \tag{8}$$

is the relative flux of longitudinal virtual photons (sometimes referred to as the virtual photon polarization). Since Γ and ϵ are purely kinematic factors, it is convenient to define the reduced cross section

$$\sigma_r = \frac{1}{\Gamma}\frac{d\sigma}{d\Omega dE'} = \sigma_T(W^2, Q^2) + \epsilon\sigma_L(W^2, Q^2). \tag{9}$$

All the hadronic structure information is therefore, contained in σ_T and σ_L, which are only dependent on W^2 and Q^2. In the $Q^2 = 0$ limit $\sigma_T(\nu, Q^2)$ should be equal to the measured photo-absorption cross section[14–18] $\sigma_\gamma(\nu)$ for real photons (here ν is the energy of the photon).

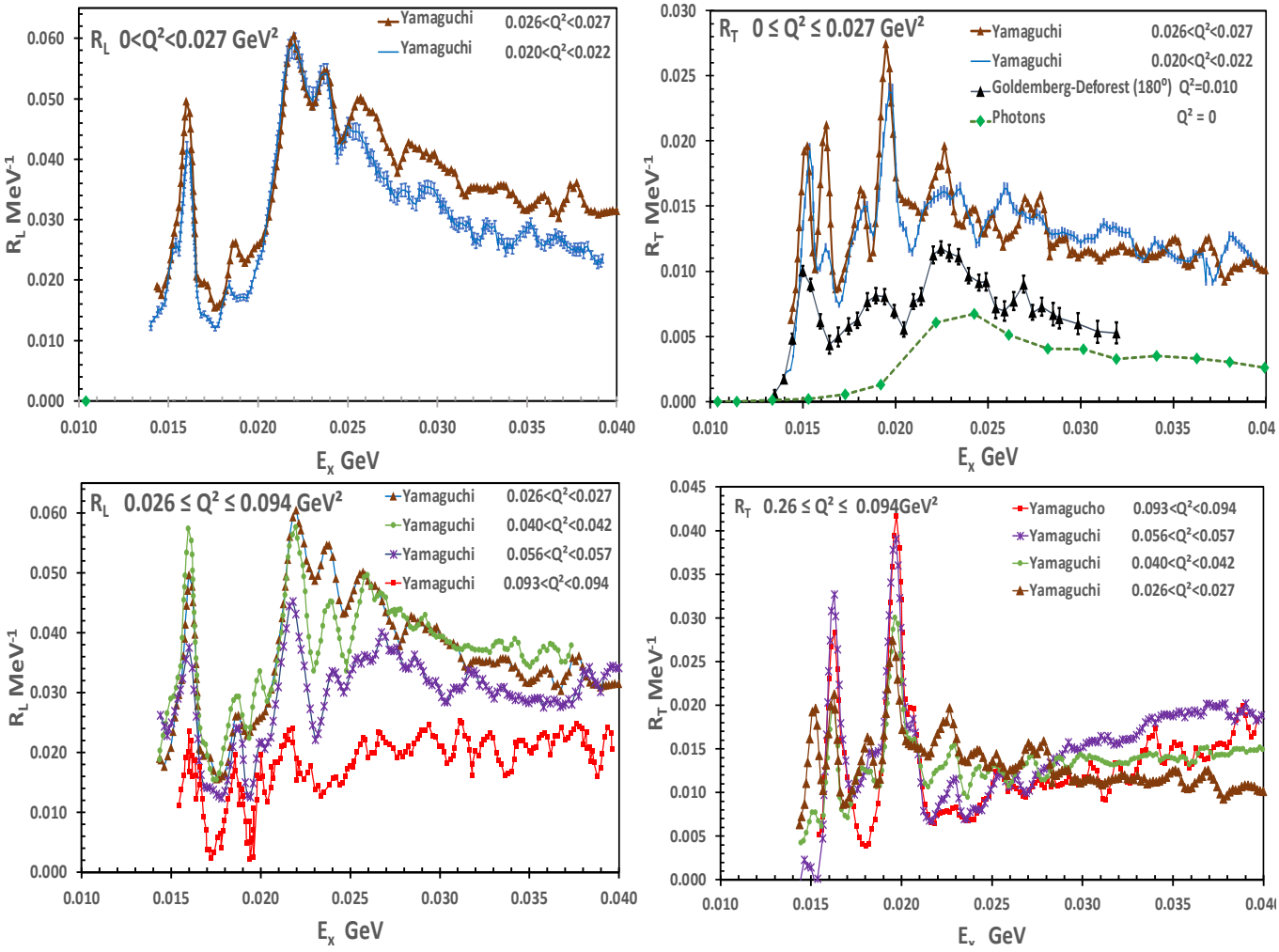

FIG. 3: Extractions of $\mathcal{R}_L$ and $\mathcal{R}_T$ in the nuclear excitation region (16< E_x < 40 MeV). The measurements are from Yamaguchi:71[6] except for $\mathcal{R}_T(Q^2 = 0)$ which we extract from photo-absorption data, and $\mathcal{R}_T(Q^2 = 0.01)$ which we extract from electron scattering cross section measurements at 180^0 (published by Goldemberg:64 [19] and Deforest:65 [20]).

B. Description in terms of structure functions

This description is primarily used in the inelastic continuum region. In the one-photon-exchange approximation, the spin-averaged cross section for inclusive electron-proton scattering can be expressed in terms of two structure functions as follows

$$\frac{d\sigma}{d\Omega dE'} = \sigma_M[\mathcal{W}_2(W^2,Q^2) + 2\tan^2(\theta/2)\mathcal{W}_1(W^2,Q^2)]$$
$$\sigma_M = \frac{\alpha^2\cos^2(\theta/2)}{[2E_0 sin^2(\theta/2)]^2} = \frac{4\alpha^2 E'^2}{Q^4}\cos^2(\theta/2) \quad (10)$$

where σ_M is the Mott cross section, $\alpha = 1/137$ is the fine structure constant. The $\mathcal{F}_1$ and $\mathcal{F}_2$ structure functions are related to $\mathcal{W}_1$ and $\mathcal{W}_2$ by $\mathcal{F}_1 = M\mathcal{W}_1$ and $\mathcal{F}_2 = \nu\mathcal{W}_2$. The structure functions are typically expressed as functions of Q^2 and W^2, or alternatively ν and $x = Q^2/(2M\nu)$. At large Q^2 and ν (deep inelastic region) x is the fractional momentum of the nucleon carried by the quarks. At low Q^2 there are target mass corrections. The target mass scaling variable [21–23] is ξ_{TM} where,

$$\xi_{TM} = \frac{Q^2}{M\nu[1+\sqrt{1+Q^2/\nu^2}]}. \quad (11)$$

The quantity R is defined as the ratio of the virtual photo-absorption cross section σ_L/σ_T, and is related to the structure functions by,

$$R(x,Q^2) = \frac{\sigma_L}{\sigma_T} = \frac{\mathcal{F}_2}{2x\mathcal{F}_1}(1+\frac{4M^2x^2}{Q^2}) - 1 = \frac{\mathcal{F}_L}{2x\mathcal{F}_1}, \quad (12)$$

where $\mathcal{F}_L$ is called the longitudinal structure function.

where $\mathcal{F}_L$ is called the longitudinal structure function. The structure functions are expressed in terms of σ_L and σ_T as follows:

$$K = \frac{Q^2(1-x)}{2Mx} = \frac{2M\nu - Q^2}{2M} \quad (13)$$
$$\mathcal{F}_1 = \frac{MK}{4\pi^2\alpha}\sigma_T \quad (14)$$

$$\mathcal{F}_2 = \frac{\nu K(\sigma_L+\sigma_T)}{4\pi^2\alpha(1+\frac{Q^2}{4M^2x^2})} \quad (15)$$

$$\mathcal{F}_L(x,Q^2) = \mathcal{F}_2\left(1+\frac{4M^2x^2}{Q^2}\right)-2x\mathcal{F}_1, \quad (16)$$

or

$$2x\mathcal{F}_1 = \mathcal{F}_2\left(1+\frac{4M^2x^2}{Q^2}\right)-\mathcal{F}_L(x,Q^2). \quad (17)$$

In addition, $2x\mathcal{F}_1$ is given by

$$2x\mathcal{F}_1(x,Q^2) = \mathcal{F}_2(x,Q^2)\frac{1+4M^2x^2/Q^2}{1+R(x,Q^2)}, \quad (18)$$

or equivalently

$$\mathcal{W}_1(x,Q^2) = \mathcal{W}_2(x,Q^2)\times\frac{1+\nu^2/Q^2}{1+R(x,Q^2)}. \quad (19)$$

C. Description in terms of response functions

This description is primarily used in the nuclear excitation and QE regions. The electron scattering differential cross section is written in terms of longitudinal ($\mathcal{R}_L(Q^2,\nu)$) and transverse ($\mathcal{R}_T(Q^2,\nu)$) nuclear response functions [24]

$$\frac{d\sigma}{d\nu d\Omega} = \sigma_M[A\mathcal{R}_L(Q^2,\nu)+B\mathcal{R}_T(Q^2,\nu)] \quad (20)$$

where σ_M is the Mott cross section, $A=(Q^2/\mathbf{q}^2)^2$ and $B=\tan^2(\theta/2)+Q^2/2\mathbf{q}^2$.

The relationships between the nuclear response functions, structure functions and virtual photon absorption cross sections are:

$$\mathcal{R}_T(\mathbf{q},\nu) = \frac{2\mathcal{F}_1(\mathbf{q},\nu)}{M} = \frac{K}{2\pi^2\alpha}\sigma_T \quad (21)$$

$$\mathcal{R}_L(\mathbf{q},\nu) = \frac{\mathbf{q}^2}{Q^2}\frac{\mathcal{F}_L(\mathbf{q},\nu)}{2Mx} = \frac{\mathbf{q}^2}{Q^2}\frac{K}{4\pi^2\alpha}\sigma_L \quad (22)$$

Where the units of $\mathcal{R}_L(\mathbf{q},\nu)$ and $\mathcal{R}_T(\mathbf{q},\nu)$ correspond to the units of M^{-1}.

The quantity $R_{\sigma LT}$ (the ratio of the virtual photo-absorption cross section σ_L/σ_T) is related to the response functions by,

$$R_{\sigma LT}(x,Q^2)=\frac{\sigma_L}{\sigma_T}=\frac{\mathcal{F}_L}{2x\mathcal{F}_1}=\frac{2Q^2}{\mathbf{q}^2}\frac{\mathcal{R}_L(\mathbf{q},\nu)}{\mathcal{R}_T(\mathbf{q},\nu)} \quad (23)$$

The square of the electric and magnetic form factors for elastic scattering and nuclear excitations are obtained by the integration of the measured response functions over ν for each nuclear state. Typically, when form factors for *nuclear elastic scattering* and *nuclear excitations* are extracted from electron scattering data there is an additional factor of Z^2 in the definition of σ_M (where Z is the atomic number of the nucleus). However, in this paper, we treat QE scattering and nuclear excitations in the same way. Therefore, we do not include a Z^2 factor in the definition of σ_M.

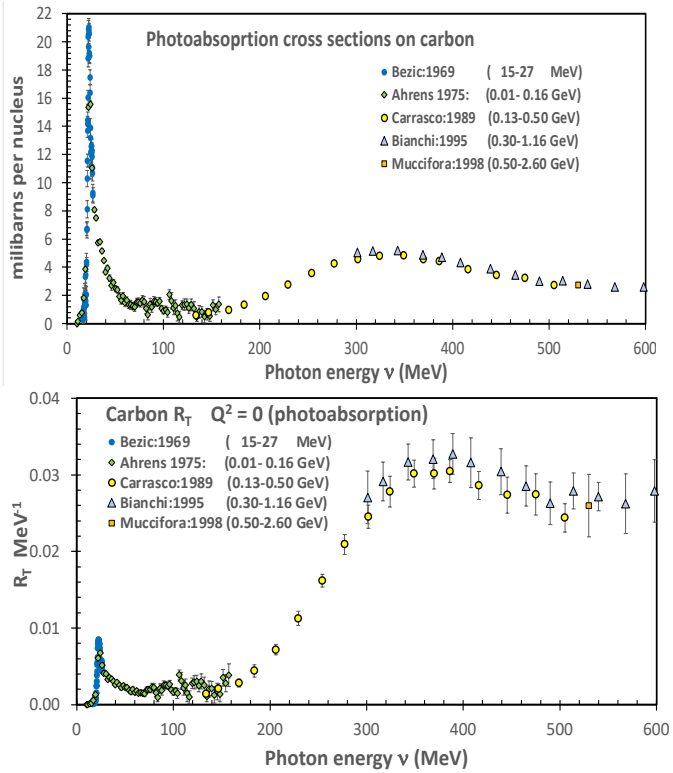

FIG. 4: Top: photo-absorption cross section as a function of photon energy ν from 0 to 0.6 GeV. Bottom: The response function $\mathcal{R}_T(Q^2=0,\nu)$ extracted from the photon cross sections.

1. *Extraction of response functions from photo-absorption cross sections*

At $Q^2=0$ the *virtual* photo-absorption cross section is equal to the photo-absorbtion cross section for *real* photons. Therefore $\mathcal{R}_L(Q^2=0,\nu)$ and $\mathcal{R}_T(Q^2=0,\nu)$ are given by

$$\mathcal{R}_L(Q^2=0,\nu) = \frac{\nu^3}{4\pi^2\alpha}\lim_{Q^2\to 0}\left[\frac{\sigma_L(Q^2)}{Q^2}\right]$$

$$\mathcal{R}_T(Q^2=0,\nu) = \frac{\nu}{2\pi^2\alpha}\sigma_\gamma(\nu), \quad (24)$$

where $\sigma_\gamma(\nu)$ is the photo-absorption cross section for photons of energy ν on a carbon nucleus.

The measured photo-absorption cross section[14–18] for real photons as a function of photon energy ν from 0 to 0.6 GeV is shown the top panel of Fig.4. The response function $\mathcal{R}_T(Q^2=0,\nu)$ extracted from the photo-absorption cross section is shown on the bottom panel. If the nuclear response functions are are extracted for fixed values of $\mathbf{q}$ then, since $Q^2=\mathbf{q}^2-\nu^2$, the maximum values of E_x and ν are $E_x^{max}=\nu^{max}=\mathbf{q}$ and

$$\mathcal{R}_T(\mathbf{q},\nu=\mathbf{q}) = \frac{\mathbf{q}}{2\pi^2\alpha}\sigma_\gamma(\mathbf{q}). \quad (25)$$

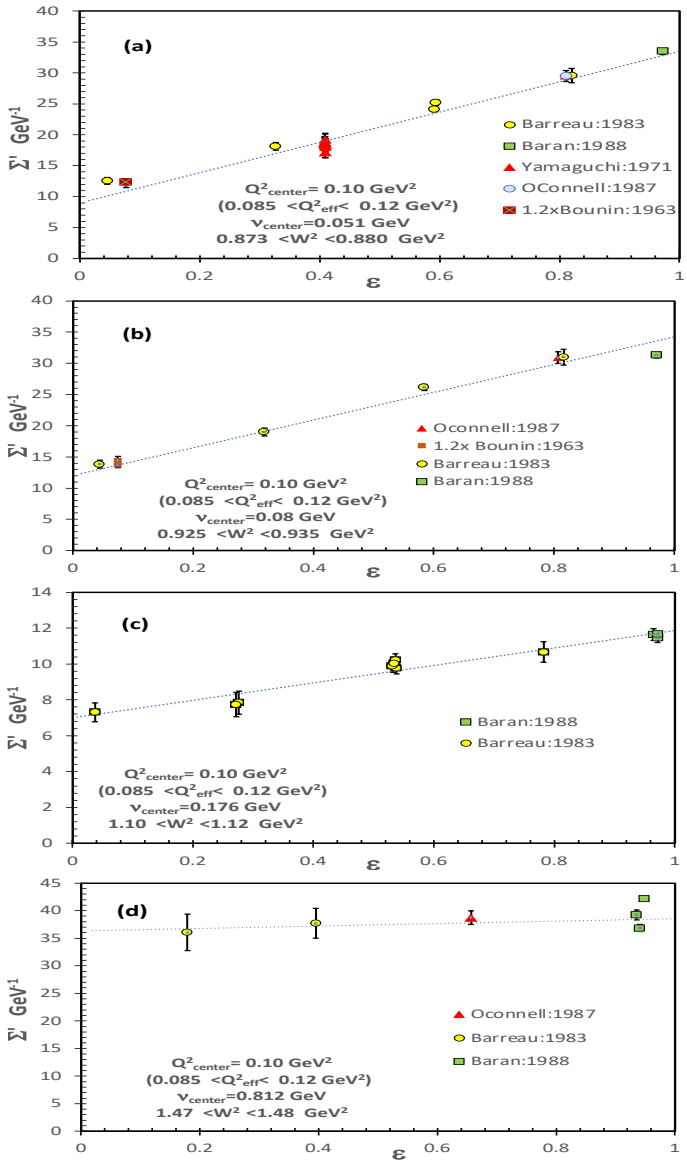

FIG. 5: Sample RL RT plots.

D. Experimental extraction of response functions

The method[8, 9] used to separate $\mathcal{R}_L(Q^2,\nu)$ and $\mathcal{R}_T(Q^2,\nu)$ is described below. The quantity

$$\begin{aligned}\Sigma(Q^2,\nu) &= H\frac{d\sigma}{d\nu d\Omega} \qquad (26)\\ &= \epsilon\mathcal{R}_L(Q^2,\nu)+\frac{1}{2}(\frac{\mathbf{q}}{Q})^2\mathcal{R}_T(Q^2,\nu)\\ H &= [\frac{1}{\sigma_M}\epsilon(\frac{\mathbf{q}}{Q})^4]\\ &= \frac{\mathbf{q}^4}{4\alpha^2E'^2}\frac{1}{\cos^2(\theta/2)+2(\frac{\mathbf{q}}{Q})^2\sin^2(\theta/2)} \qquad (27)\end{aligned}$$

is plotted as a function of the virtual photon polarization ϵ. The virtual photon polarization ϵ varies from 0 to 1 as the scattering angle θ ranges from 180 to 0 degrees. We use equation 27 for H because it is valid for all scattering angles including 180 degrees. Here, $\mathcal{R}_L(Q^2,\nu)$ is the slope, and $\frac{1}{2}\frac{\mathbf{q}^2}{Q^2_{eff}}\mathcal{R}_T(Q^2,\nu)$ is the intercept of the linear fit, When Coulomb corrections are included, the above expressions are modified as described below.

E. Electron scattering at 180^o

Including Coulomb corrections described below, the response function $\mathcal{R}_T(Q^2_{eff},\nu)$ can be extracted directly from the electron scattering cross section at 180^o.

$$\mathcal{R}_T(Q^2_{eff},\nu) = [\frac{E_0}{E_0+V_{eff}}]^2\times\frac{{Q_{eff}}^4}{4\alpha^2E'^2_{eff}}\frac{d\sigma}{d\nu d\Omega} \qquad (28)$$

F. $\mathcal{R}_L$ and $\mathcal{R}_T$ in the nuclear excitation region

As mentioned earlier In this paper, for the nuclear excitation region $< 6 < E_x < 40$ MeV we use the precise ($\pm$3%) Yamaguchi measurements of $\mathcal{R}_L$ and $\mathcal{R}_T$. For E_x <16 MeV we extract $\mathcal{R}_L$ and $\mathcal{R}_T$ from our overall fits [13] to the nuclear excitation form factors(shown as the red solid line in Figure 1). For E_x >30 MeV. we extract $\mathcal{R}_L$ and $\mathcal{R}_T$ from our analysis of all available electron scattering data as described below. In the nuclear excitation region we extract $\mathcal{R}_T$ for Q^2=0 from measured photo-absorption cross sections. We extract $\mathcal{R}_T$ for Q^2 = 0.01 GeV^2 from electron scattering cross sections at E_0= 55 and 70 MeV and θ=180^0 published in Goldemberg:64 [19] and electron scattering cross sections at E_0 =65 MeV and θ =180^0 published in Deforest:65 [20].

III. COULOMB CORRECTIONS

In modeling QE and inelastic (pion production) scattering from bound nucleons, Coulomb corrections to QE and inelastic pion production processes are taken into account using the "Effective Momentum Approximation"(EMA) [25, 26]. The approximation is a simple energy gain/loss method, using a slightly higher incident and scattered electron energies at the vertex than measured in the lab. The effective incident energy is $E_{eff} = E_0 + V_{eff}$, and the effective scattered energy is $E'_{eff} = E' + V_{eff}$.

Assuming a spherical charge distribution in the nucleus (of radius R) the electrostatic potential inside the charged sphere can be defined as followed:

$$V(r) = \frac{3\alpha(Z-1)}{2R} + \frac{\alpha(Z-1)}{2R}\frac{r}{R} \qquad (29)$$

where R (in units of GeV) is given by:

$$R = 1.1A^{(1/3)} + 0.86A^{(-1/3)}. \qquad (30)$$

$$V_{eff} = +0.775V(r=0) = 0.775\ \frac{3}{2}\ \alpha(Z-1)/R \quad (31)$$

where Z and A are the atomic number and atomic weight of the nucleus, respectively.

In this analysis we use V_{eff}**= 3.1 ± 0.25 MeV** extracted from a comparison of positron and electron QE scattering cross sections on carbon[26]. Including Coulomb corrections we define:

$$E_{0,eff} = E_0 + V_{eff} \quad (32)$$
$$E'_{eff} = E' + V_{eff} \quad (33)$$
$$\nu_{eff} = \nu \quad (34)$$
$$Q^2_{eff} = 4(E_0 + V_{eff})(E' + V_{eff})\sin^2(\theta/2) \quad (35)$$
$$\mathbf{q_{eff}}^2 = Q^2_{eff} + \nu^2 \quad (36)$$
$$W^2_{eff} = M^2 + 2M\nu - Q^2 eff \quad (37)$$

The response functions are calculated with $Q^2 = Q^2_{eff}$ and $E' = E'_{eff}$. In addition, there is a focusing factor $F^2_{foc} = \left[\frac{E_0+V_{eff}}{E_0}\right]^2$ which modifies the Mott cross section. The modified Mott cross section is

$$\sigma_{M-eff} = F^2_{foc}\frac{\alpha^2\cos^2(\theta/2)}{[2E_{eff}\sin^2(\theta/2)]^2}$$

Therefore

$$\epsilon^{CC} = \left[1 + 2(1+\frac{\nu^2}{Q^2_{eff}})\tan^2\frac{\theta}{2}\right]^{-1} \quad (38)$$

$$\Sigma'(Q^2_{eff},\nu) = H^{CC}\frac{d\sigma}{d\nu d\Omega} \quad (39)$$
$$= \epsilon\mathcal{R}_L(Qeff^2,\nu) + \frac{1}{2}(\frac{\mathbf{q_{eff}}}{Q_{eff}})^2\mathcal{R}_T(Q^2_{eff},\nu)$$

$$H^{CC} = \left[\frac{E_0}{E_0+V_{eff}}\right]^2 \times \frac{\mathbf{q_{eff}}^4}{4\alpha^2 E'^2_{eff}}\frac{1}{\cos^2(\theta/2) + 2(\frac{\mathbf{q_{eff}}}{Q_{eff}})^2\sin^2(\theta/2)} \quad (40)$$

In this analysis bin-centering correction factors are determined using an overall fit to model all existing electron scattering data on ^{12}C. As mentioned above, the fit includes the following components: (a) Nuclear-elastic scattering and excitation of nuclear states, (b) QE scattering and (c) Resonance production and the inelastic continuum. The parameterizations of the form factors for nuclear-elastic scattering and excitation of nuclear states are presented in [13]. A brief description of the QE and resonance production fits and the measurement of the Coulomb Sum Rule are presented in [12].

IV. EXTRACTIONS OF R_L AND R_T

We extract the response functions in bins of $\mathbf{q}$ as well as bins in Q^2 (shown in Table I as a function of the energy transfer ν. However for low excitation energy ($E_x < 50$ MeV) the bin centering corrections are minimized if we extract the response functions as functions of excitation energy. Similarly for ($E_x > 50$ MeV) the bin centering corrections are minimized if we extract the response functions as functions the square of the final state invariant mass W^2. Therefore, we extract the response functions both as functions of E_x and W^2. For fixed values of Q^2 (or $\mathbf{q}$) the results can then be plotted versus E_x, ν, or W^2 using the following expressions.

$$\nu = E_x + \frac{Q^2}{2M_A}$$
$$W^2 = M^2 + 2M\nu - Q^2\mathbf{q} = Q^2 + \nu^2$$

where M_A is the mass of the nuclear target (for carbon $M_{A=12}$=11.178 GeV). For fixed values of $\mathbf{q}$ the energy transfer ν can be extracted from E_x by solving the following quadratic equation

$$\nu = E_x + (\mathbf{q}^2 + \nu^2)/(2M_A$$

and then using equation 41 with $Q^2 = \mathbf{q}^2 + \nu^2$.

We apply bin centering corrections as well as normalization corrections to each data set to account for the small difference in the normalizations (within the quoted errors) of each data set. We then perform a (Rosenbluth) linear fit for the data in each Q^2 and ν (or $\mathbf{q}$ and ν) bin. Here $\mathcal{R}_L(Q^2_{eff},\nu$ is the slope, and $\frac{1}{2}\frac{\mathbf{q_{eff}}^2}{Q^2_{eff}}\mathcal{R}_T(Q^2_{eff},\nu)$ is the intercept of the linear fit.

A. Summary of corrections to the data

We use our cross section fit (σ_{model}) to evaluate the following corrections to the cross sections in each bin in Q^2, ν (or $\mathbf{q}, \nu$).

1. From the overall fit we extract the relative normalization (N_i) of the various data sets as given in Table II,

2. We use the fit to apply bin centering corrections (C_i) to all extracted value off Σ'_i that are within the Q^2_{eff} range for each Q^2, ν bin such that they reflect the values at Q^2_{center}, $\nu_{x-center}$ for each cross section measurement in each bin.

$$C_i = \frac{\epsilon\mathcal{R}^{fit}_{L-center} + \frac{1}{2}(\frac{\mathbf{q_{center}}}{Q_{center}})^2\mathcal{R}^{fit}_{T-center}}{\epsilon\mathcal{R}^{fit}_{L-data} + \frac{1}{2}(\frac{\mathbf{q_{data}}}{Q_{data}})^2\mathcal{R}^{fit}_{T-data}} \quad (41)$$

$$\mathcal{R}^{fit}_{L-center} = \mathcal{R}^{fit}_L(Q^2_{center}, X_{center})$$
$$\mathcal{R}^{fit}_{T-center} = \mathcal{R}^{fit}_T(Q^2_{center}, X_{center})$$
$$\mathcal{R}^{fit}_{L-data} = \mathcal{R}^{fit}_L(Q^2_{data}, X_{data})$$
$$\mathcal{R}^{fit}_{T-data} = \mathcal{R}^{fit}_T(Q^2_{data}, X_{data})$$

Where $X = E_x$ for $E_x < 50$ MeV, and $X = W^2$ for $E_x > 50$ MeV,

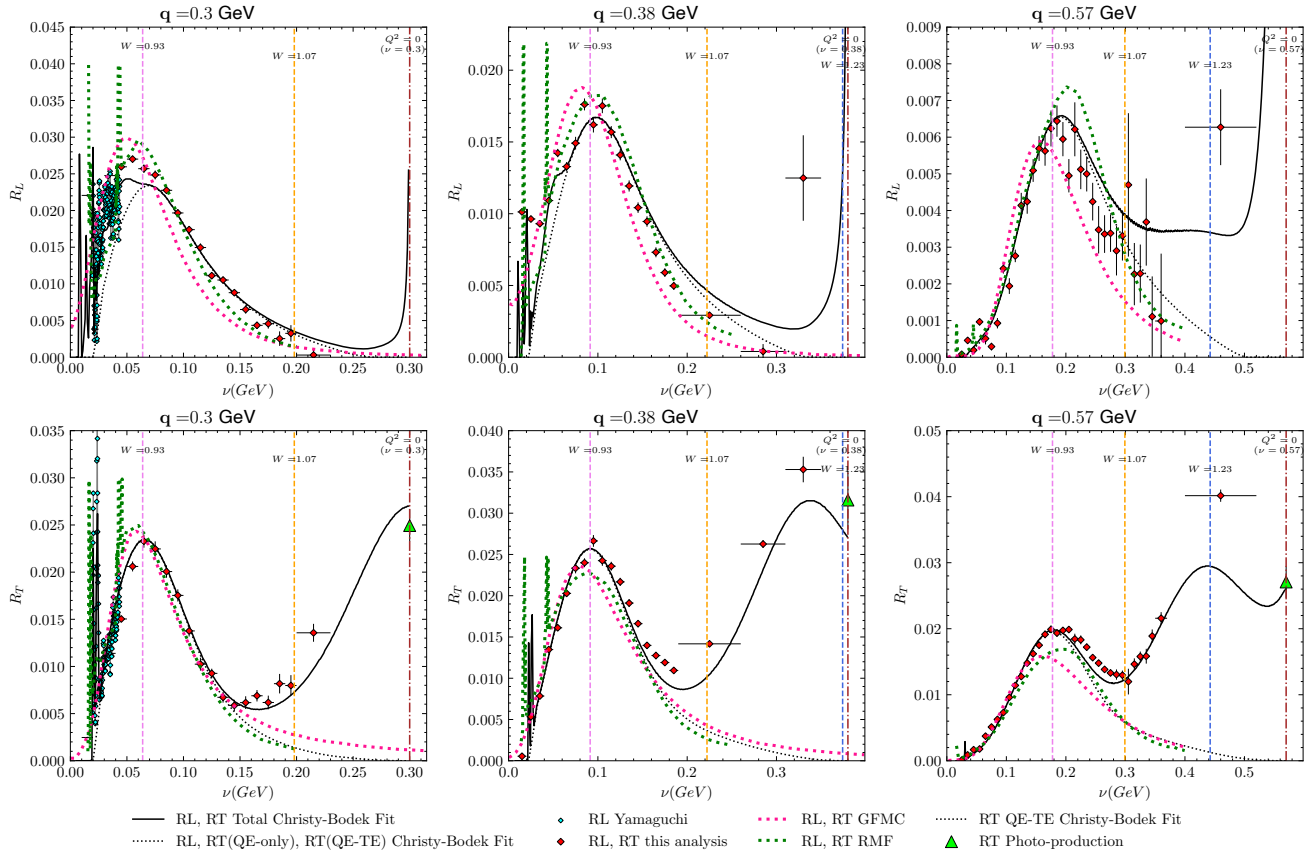

FIG. 6: Comparisons between our extraction of $\mathcal{R}_L(\mathbf{q},\nu)$ and $\mathcal{R}_T(\mathbf{q},\nu)$ in units of MeV^{-1} (red diamonds) and two theoretical calculations of the sum of 1-body and 2-body (1b+2b) contribution to the QE response functions. The GFMC[2] calculation is shown as the dotted red line and the ED-RMF[4] calculation is shown as the dotted green line. The transverse enhancement (TE) in both 1b and 2b currents is included in the total. The Christy-Bodek universal fit for the total (from all processes) is the solid black line, and the QE contribution (including TE) to the total is the dotted black line. The theoretical predictions are only available for three values of the momentum transfer $\mathbf{q}$ (0.3, 0.38 and 0.57 GeV).

B. Comparison to Theory

Comparisons between our extraction of $\mathcal{R}_L(\mathbf{q},\nu)$ and $\mathcal{R}_T(\mathbf{q},\nu)$ (in units of MeV^{-1} to two theoretical calculations (of the QE contributions only) are shown in Fig.6. In the nuclear excitation region we also show the Yamaguchi:1971[6] measurements of $\mathcal{R}_L(\mathbf{q},\nu)$ and $\mathcal{R}_T(\mathbf{q},\nu)$ for $\mathbf{q}$= 0.3 GeV. At present, the "First Principle Green's Function Monte Carlo" (GFMC)[2] calculation and the "Energy Dependent-Relativistic Mean Field" (ED-RMF)[4] calculation are only available for three values of momentum transfer $\mathbf{q}$ (0.30, 0.38, and 0.57 GeV). The two theoretical formalisms include both 1-body+2-body current (1b+2b) contributions to the 1p1h (1 particle 1 hole) QE response functions. In both models there is some enhancement of $\mathcal{R}_T^{QE}(\mathbf{q},\nu)$ if only 1b currents are included , and an additional enhancement if both 1b and 2b currents are included. Both calculations are in reasonable agreement with the measurements in the QE region. The solid black lines in Fig.6 are $\mathcal{R}_L(\mathbf{q},\nu)$ and $\mathcal{R}_T(\mathbf{q},\nu)$ from the Christy-Bodek universal fit (the QE contribution (including TE) to the total is the dotted black line).

The two theoretical calculations do not describe the measurements in te the nuclear excitation region. The GFMC calculations do not show any nuclear excitations and the ED-RMF calculations group all excitations in two fixed values of ν (which are the same for the three values of $\mathbf{q}$) as shown in Fig.6.

C. Comparison to Previous Measurements of $\mathcal{R}_L^{QE}(\mathbf{q},\nu)$ and $\mathcal{R}_T^{QE}(\mathbf{q},\nu)$

A comparison between our extraction (thick solid blue) of $\mathcal{R}_L(\mathbf{q},\nu)$ and $\mathcal{R}_T(\mathbf{q},\nu)$ and previous extractions are shown in Fig. **??**. The first extraction was published in Barreau:81[10] for the square of the 4-momentum transfer squared Q^2=0.16 GeV^2). Another extraction by the same group was published in Barreau:82[11] for $\mathbf{q}$ values of 0.30, 0.40 and 0.55 GeV. A later extraction by Jourdan:96[8, 9] was also one for 3 values of momentum

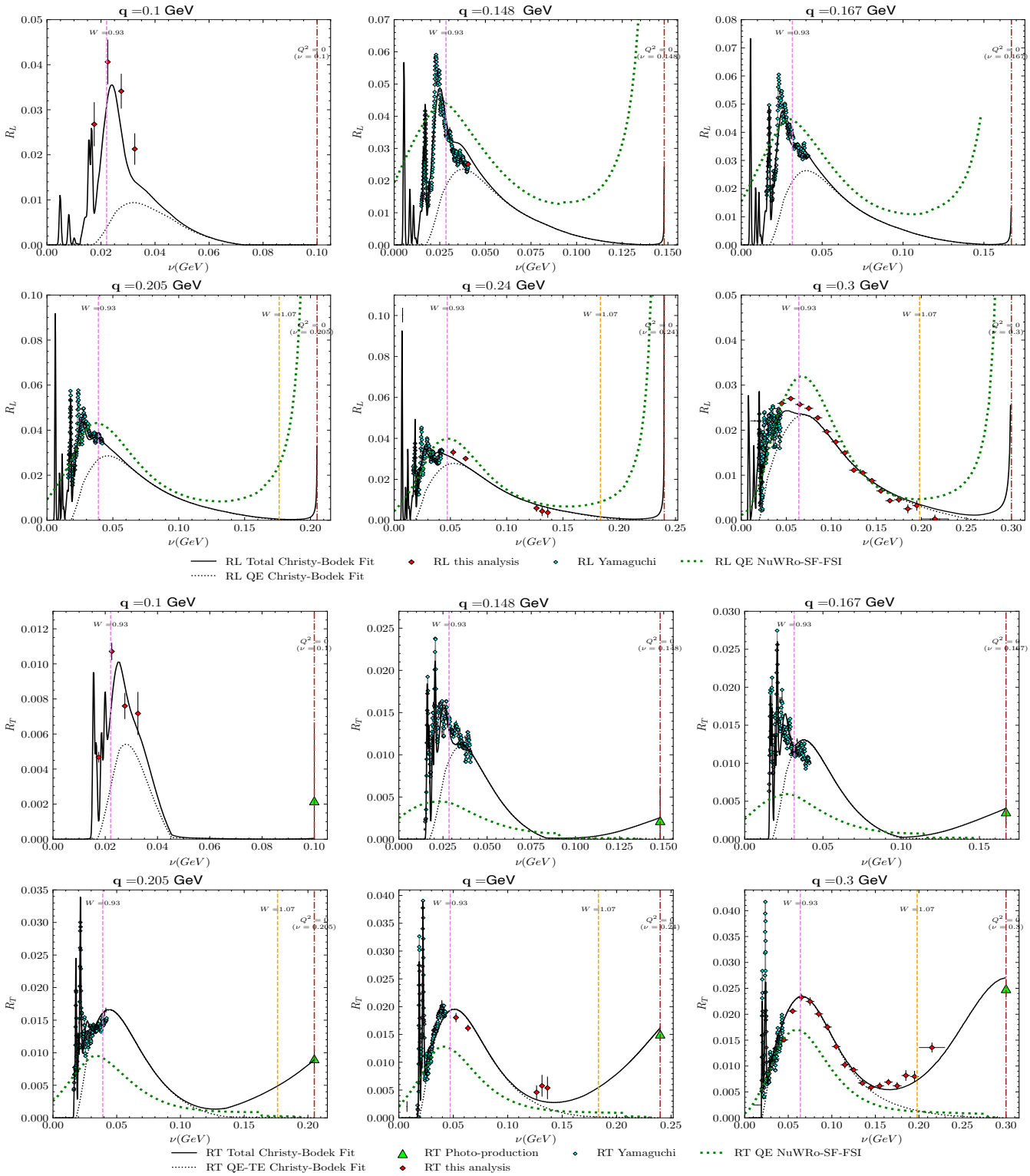

FIG. 7: Our extractions of $\mathcal{R}_L$ and $\mathcal{R}_T$ for $0.1 \leq \mathbf{q} \leq 0.300$ GeV versus ν. In the nuclear excitation region we also show measurements from Yamaguchi:1971[6], and $\mathcal{R}_T(\mathbf{q} = 0.01)$ GeV extracted from electron scattering cross sections at 180^0 published in Goldemberg:64 [19] and in Deforest:65 [20]. The values of $\mathcal{R}_T(\mathbf{q} = \nu)$ are extracted from photo-absorption data.

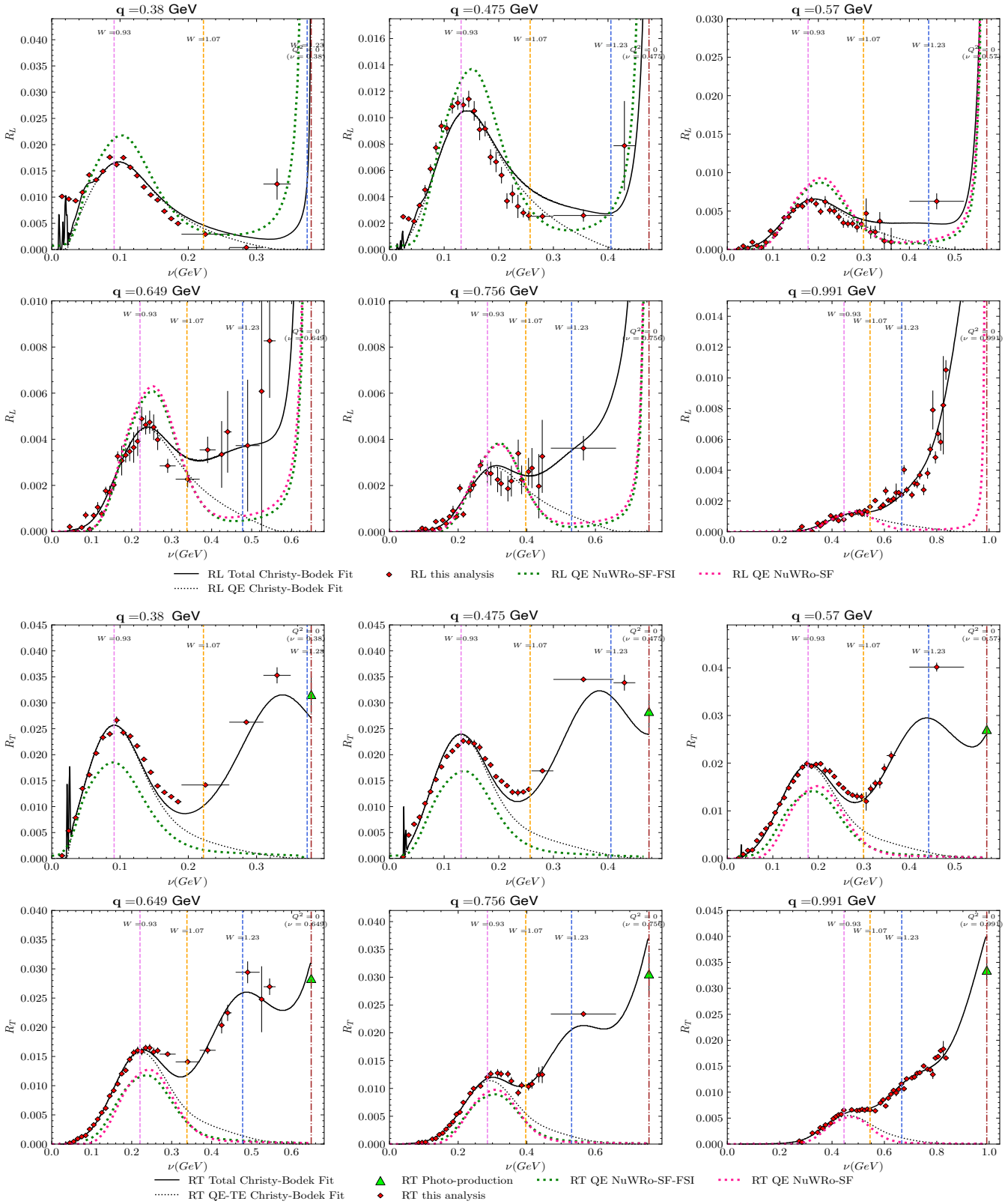

FIG. 8: Same as Fig. 7 for $0.38 \leq \mathbf{q} \leq 0.99$ GeV versus ν.

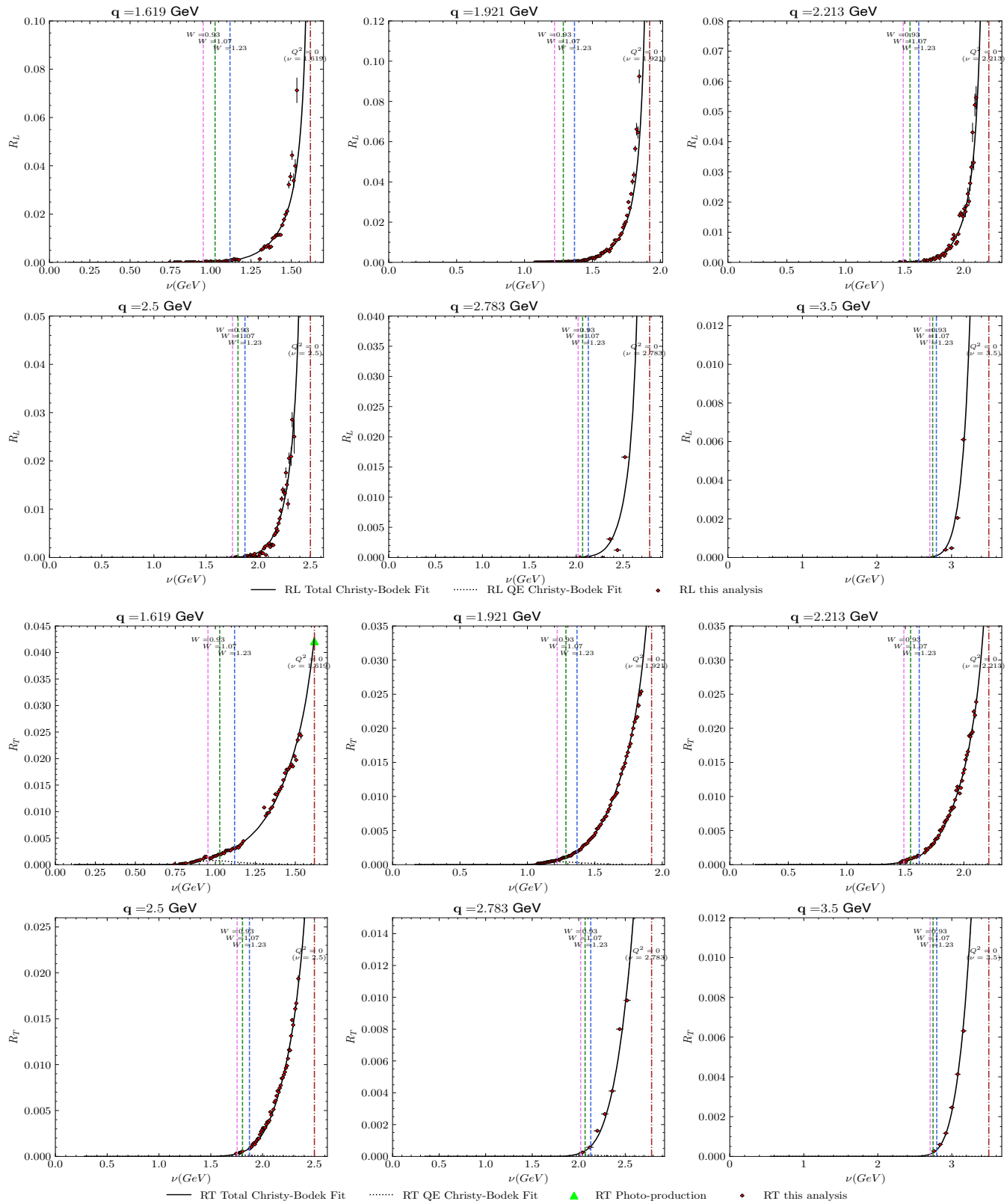

FIG. 9: Same as Fig. 7 for $1.6 \leq \mathbf{q} \leq 3.5$ GeV versus ν.

transfer (**q**=0.30, 0.38 and 0.57 GeV). It that analysis the same Barreau:82 data was used with some additional Saclay. data Our extraction is more extensive because we our data sample is much larger (as summarized in Table II.

D. Results for fixed values of 0.1 < q < 3.75 GeV

Our extractions of $\mathcal{R}_L$ and $\mathcal{R}_T$ for **q** values of 0.1, 0.148, 0.167, 0.205, 0.24 and 0.30 versus ν are shown in Fig 7. In the nuclear excitation region we also show measurements from Yamaguchi:1971[6], and $\mathcal{R}_T(\mathbf{q} = 0.01)$ GeV extracted from electron scattering cross sections at 180^0 published in Goldemberg:64 [19] and in Deforest:65 [20]. the values $\mathcal{R}_T(\nu = |\mathbf{q}|$ are extracted from photo-absorption data.

Our extractions of $\mathcal{R}_L$ and $\mathcal{R}_T$ for $0.30 \leq \mathbf{q} \leq 0.475$ GeV versus excitation energy are shown in Fig 8. In the nuclear excitation region we show high resolution extractions from Yamaguchi:1971[6]. In the QE region we compare to extractions published in Jourdan:96[8, 9] and Barreau:81[10]. We also show values of $\mathcal{R}_T(\mathbf{q})$ extracted from electron scattering cross sections at 180^0 published in Ryan:84[7]. The values of $\mathcal{R}_L(\mathbf{q} = E_x)$ are zero and the values of $\mathcal{R}_T(\mathbf{q} = E_x)$ are extracted from photo-absorption data.

Our extractions of $\mathcal{R}_L$ and $\mathcal{R}_T$ for **q**=0.655 and **q**=0.765 GeV are shown in Fig 9. The values of $\mathcal{R}_L(\mathbf{q} = E_x)$ are zero and the values of $\mathcal{R}_T(\mathbf{q} = E_x)$ are extracted from photo-absorption data.

E. Results for fixed values of Q^2

THE PLOTS ARE PLACE HOLDERS

Our extractions of $\mathcal{R}_L$ and $\mathcal{R}_T$ for $0.0 \leq \mathbf{q} \leq 0.026$ GeV^2 versus excitation energy E_x are shown in Fig 10 In the nuclear excitation region we also show measurements from Yamaguchi:1971[6], and $\mathcal{R}_T(\mathbf{q} = 0.01)$ GeV extracted from electron scattering cross sections at 180^0 published in Goldemberg:64 [19] and in Deforest:65 [20].

Our extractions of $\mathcal{R}_L$ and $\mathcal{R}_T$ for $0.026 \leq \mathbf{q} \leq 0.12$ GeV versus excitation energy are shown in Fig 11. In the nuclear excitation region we show high resolution extractions from Yamaguchi:1971[6]. In the QE region we compare to extractions published in Jourdan:96[8, 9] and Barreau:81[10]. We also show values of $\mathcal{R}_T(\mathbf{q})$ extracted from electron scattering cross sections at 180^0 published in Ryan:84[7]. The values of $\mathcal{R}_L(\mathbf{q} = E_x)$ are zero and the values of $\mathcal{R}_T(\mathbf{q} = E_x)$ are extracted from photo-absorption data.

Our extractions of $\mathcal{R}_L$ and $\mathcal{R}_T$ for **q**=0.765 GeV are shown in Fig 12. The values of $\mathcal{R}_L(\mathbf{q} = E_x)$ are zero and the values of $\mathcal{R}_T(\mathbf{q} = E_x)$ are extracted from photo-absorption dat

F. Acknowledgments

Research supported in part by the U.S. Department of Energy under University of Rochester grant number DE-SC0008475, and the Office of Science, Office of Nuclear Physics under contract DE-AC05-06OR23177.

Appendix A EXTRACTION OF $R_{\sigma LT}(Q^2, \nu) = \sigma_L/\sigma_T$

The ratio of the virtual photo-absorbption cross sections $R_{\sigma LT}(Q^2, \nu) = \sigma_L/\sigma_T$ can be obtained from the extracted values of $\mathcal{R}_L(Q^2, \nu)$ and $\mathcal{R}_T(Q^2, \nu)$ using equation 23. However In order to properly account for the correlations in the uncertainties in of $\mathcal{R}_L(Q^2, \nu)$ and $\mathcal{R}_T(Q^2, \nu)$ we redo the analysis using the following equation:

$$\begin{aligned} \Sigma''(Q^2_{eff}, \nu) &= G^{CC} \frac{d\sigma}{d\nu d\Omega} \\ &= \epsilon \mathcal{R}_L(Qeff^2, \nu) + \frac{1}{2}(\frac{\mathbf{q_{eff}}}{Q_{eff}})^2 \mathcal{R}_T(Q^2_{eff}, \nu) \end{aligned} \tag{42}$$

where

$$G^{CC} = \big[\frac{Q^2_{eff}}{\mathbf{q_{eff}}}\big]^2 H^{CC}$$

A Investigation of "Transverse Enhancement" and "Longitudinal Suppression"

THIS SECTION IS NOT FINISHED YET

1 Elastic electron-nucleon scattering

In the case of elastic scattering from free nucleons ($x = Q^2/2M\nu$=1) the structure functions are related to the nucleon form factors by the following expressions:

$$\mathcal{W}^{elastic}_{1p} = \delta(\nu - \frac{Q^2}{2M})\tau |G_{Mp}(Q^2)|^2$$

$$\mathcal{W}^{elastic}_{1n} = \delta(\nu - \frac{Q^2}{2M})\tau |G_{Mn}(Q^2)|^2$$

and

$$\mathcal{W}^{elastic}_{2p} = \delta(\nu - \frac{Q^2}{2M}) \frac{[G_{Ep}(Q^2)]^2 + \tau [G_{Mp}(Q^2)]^2}{1+\tau}$$

$$\mathcal{W}^{elastic}_{2n} = \delta(\nu - \frac{Q^2}{2M}) \frac{[G_{En}(Q^2)]^2 + \tau [G_{Mn}(Q^2)]^2}{1+\tau}$$

$$R^{elastic}_{p,n}(x = 1, Q^2) = \frac{\sigma^{elastic}_L}{\sigma^{elastic}_T} = \frac{4M^2}{Q^2} \left(\frac{G^2_E}{G^2_M} \right)$$

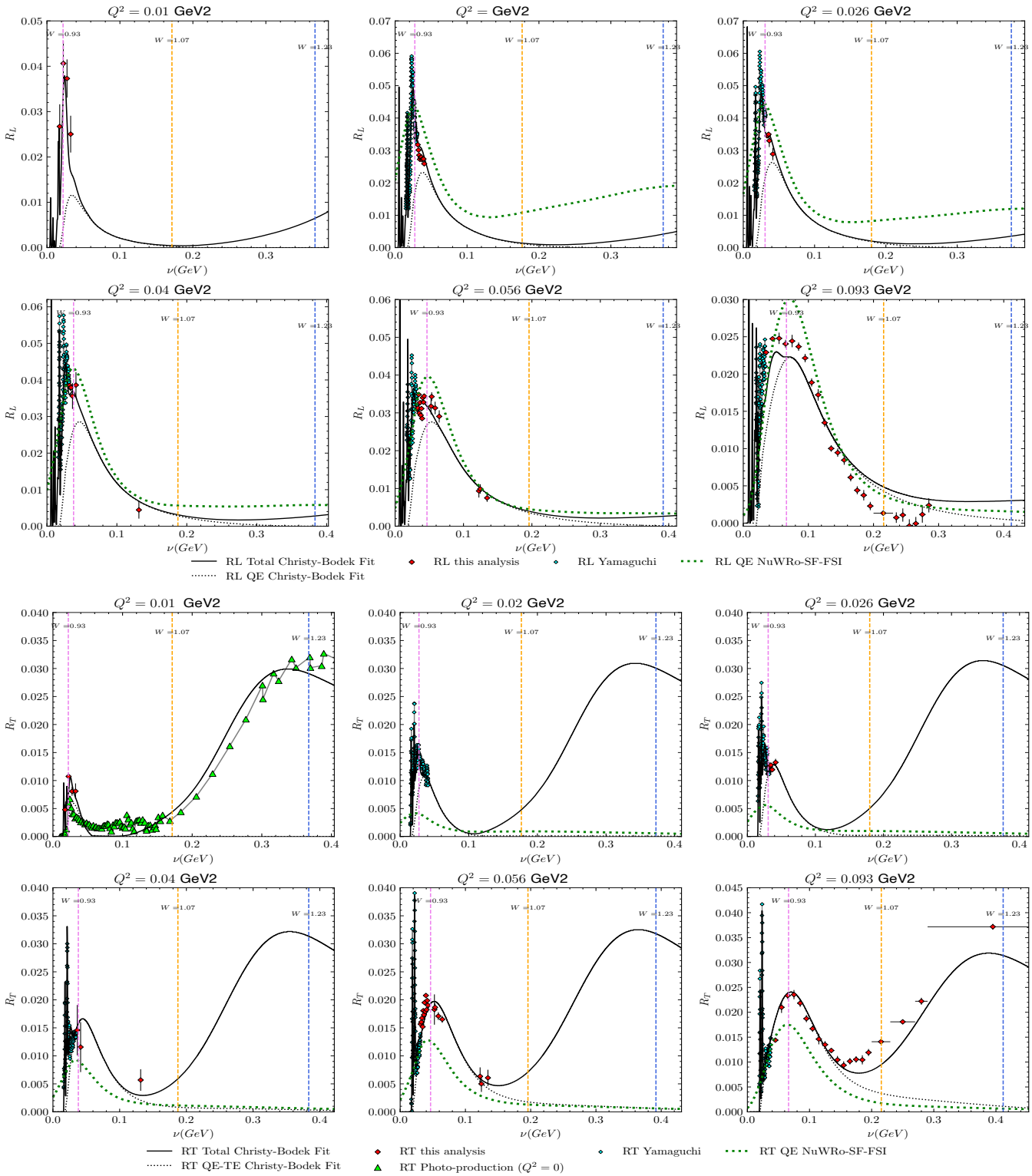

FIG. 10: Our extractions of $\mathcal{R}_L$ and $\mathcal{R}_T$ for $0.01 \leq Q^2 \leq 0.10$ GeV^2 versus ν. In the nuclear excitation region we also show measurements from Yamaguchi:1971[6], and $\mathcal{R}_T(\mathbf{q} = 0.01)$ GeV extracted from electron scattering cross sections at 180^0 published in Goldemberg:64 [19] and in Deforest:65 [20]. The values of $\mathcal{R}_T(Q^2) = 0$ are extracted from photo-absorption data.

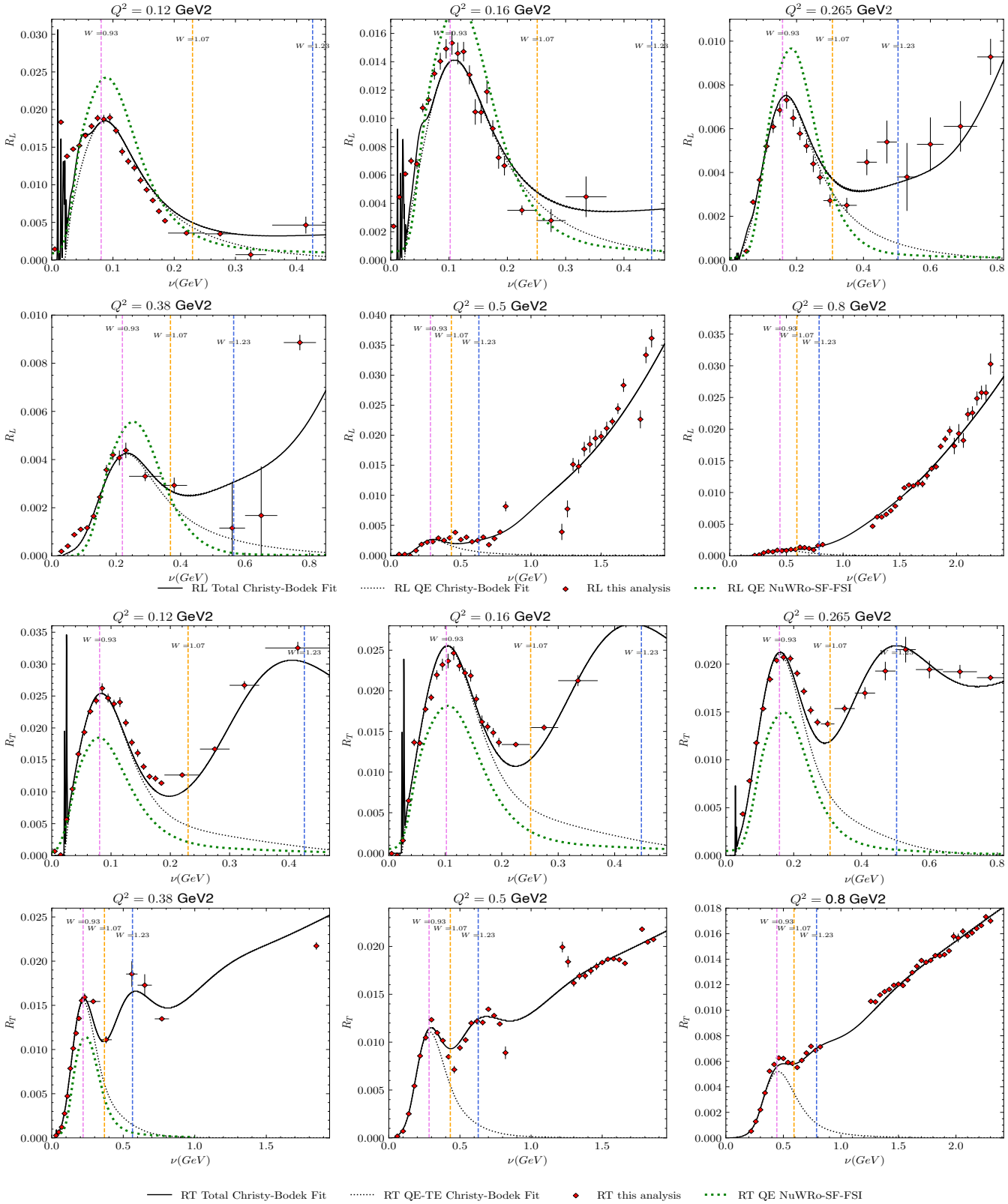

FIG. 11: Same as Fig. 10 for $0.12 \leq \mathbf{q} \leq 0.65$ GeV versus ν.

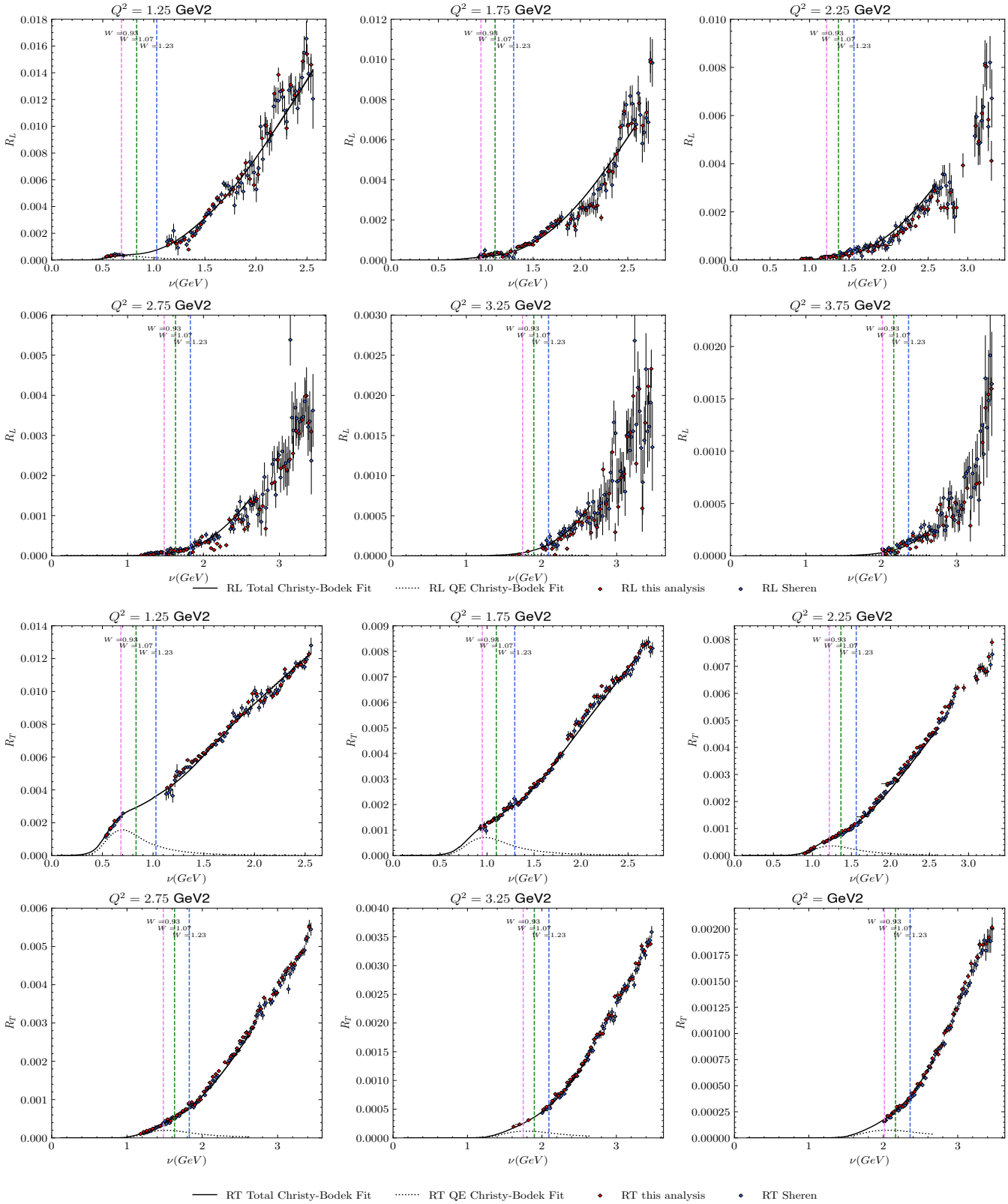

FIG. 12: Same as Fig. 10 for $1.25 \leq \mathbf{q} \leq 3.75$ GeV versus ν.

Here, $\tau = Q^2/4M_{p,n}^2$, where $M_{p,n}$ are the masses of proton and neutron. Therefore, G_{Mp} and G_{Mn} contribute to the transverse virtual photo-absorption cross section, and G_{Ep} and G_{En} contribute to the longitudinal cross section. The sum of the neutron and proton elastic response functions, and structure functions is given by:

$$\begin{aligned}\mathcal{R}_T^{N+P}(\mathbf{q},\nu) &= 2\tau[G_{Mp}(Q^2)]^2 \\ &= \frac{Q^2}{2M_p^2}\left[[G_{Mp}(Q^2)]^2 + [G_{Mn}(Q^2)]^2\right] \\ \mathcal{R}_L^{N+P}(\mathbf{q},\nu) &= \frac{\mathbf{q^2}}{Q^2}\left[[G_{Ep}(Q^2)]^2 + [G_{En}(Q^2)]^2\right]. \quad (43)\end{aligned}$$

And the ratio of the corresponding virtual photo-absorption cross section is:

$$\begin{aligned}R_{\sigma LT}^{N+P}x, Q^2) &= \frac{2Q^2}{\mathbf{q}^2}\frac{\mathcal{R}_L(\mathbf{q},\nu)}{\mathcal{R}_T(\mathbf{q},\nu)} \quad (44) \\ &= \frac{4M^2}{Q^2}\frac{[G_{Ep}(Q^2)]^2 + [G_{En}(Q^2)]^2}{[G_{Mp}(Q^2)]^2 + [G_{Mn}(Q^2)]^2}.\end{aligned}$$

[1] B. Mihaila and J. Heisenberg, Phys. Rev. Lett. **84**, 1403 (2000), arXiv:nucl-th/9910007 .
[2] A. Lovato, S. Gandolfi, J. Carlson, S. C. Pieper, and R. Schiavilla, Phys. Rev. Lett. **117**, 082501 (2016), arXiv:1605.00248 [nucl-th] .
[3] I. C. Cloët, W. Bentz, and A. W. Thomas, Phys. Rev. Lett. **116**, 032701 (2016), arXiv:1506.05875 [nucl-th] .
[4] T. Franco-Munoz, R. González-Jiménez, and J. M. Udias, "Effects of two-body currents in the one-particle one-hole electromagnetic responses within a relativistic mean-field model," (2022), arXiv:2203.09996 [nucl-th] .
[5] J. E. Sobczyk, B. Acharya, S. Bacca, and G. Hagen, Phys. Rev. C **102**, 064312 (2020), arXiv:2009.01761 [nucl-th] .
[6] A. Yamaguchi, T. Terasawa, K. Nakahara, and Y. Torizuka, Phys. Rev. C **3**, 1750 (1971).
[7] P. J. Ryan, J. B. Flanz, R. S. Hicks, B. Parker, and G. A. Peterson, Phys. Rev. C **29**, 655 (1984).
[8] J. Jourdan, Nucl. Phys. A **603**, 117 (1996).
[9] J. Jourdan, Phys. Lett. B **353**, 189 (1995).
[10] P. Barreau *et al.*, Nucl. Phys. A **358**, 287C (1981).
[11] P. Barreau *et al.*, Nucl. Phys. **A402**, 515 (1983).
[12] A. Bodek and M. E. Christy, Phys. Rev. C **106**, L061305 (2022), arXiv:2208.14772 [hep-ph] .
[13] A. Bodek and M. E. Christy, "Contribution of Nuclear Excitation Electromagnetic Form Factors in ^{12}C and ^{16}O to the Coulomb Sum Rule. arXiv: 2301.05650[nucl-th]," (2023), arXiv:2301.05650 [nucl-th] .
[14] N. Bezić, D. Brajnik, D. Jamnik, and G. Kernel, Nucl. Phys. A **128**, 426 (1969).
[15] J. Ahrens *et al.*, Nucl. Phys. A **251**, 479 (1975).
[16] R. C. Carrasco and E. Oset, Nucl. Phys. A **536**, 445 (1992).
[17] N. Bianchi *et al.*, Phys. Rev. C **54**, 1688 (1996).
[18] V. Muccifora *et al.*, Phys. Rev. C **60**, 064616 (1999), arXiv:nucl-ex/9810015 .
[19] J. Goldemberg and W. C. Barber, Phys. Rev. **134**, B963 (1964).
[20] T. Deforest, J. Walecka, G. Vanpraet, and W. Barber, Physics Letters **16**, 311 (1965).
[21] O. Nachtmann, Nucl. Phys. B **63**, 237 (1973).
[22] H. Georgi and H. D. Politzer, Phys. Rev. D **14**, 1829 (1976).
[23] R. Barbieri, J. R. Ellis, M. K. Gaillard, and G. G. Ross, Nucl. Phys. B **117**, 50 (1976).
[24] J. A. Caballero, M. C. Martinez, J. L. Herraiz, and J. M. Udias, Phys. Lett. B **688**, 250 (2010), arXiv:0912.4356 [nucl-th] .
[25] A. Aste, C. von Arx, and D. Trautmann, Eur. Phys. J. A **26**, 167 (2005), arXiv:nucl-th/0502074 .
[26] P. Gueye *et al.*, Phys. Rev. C **60**, 044308 (1999).
[27] R. Rosenfelder, Annals Phys. **128**, 188 (1980).
[28] J. S. O'Connell *et al.*, Phys. Rev. **C35**, 1063 (1987).
[29] R. M. Sealock *et al.*, Phys. Rev. Lett. **62**, 1350 (1989).
[30] D. T. Baran *et al.*, Phys. Rev. Lett. **61**, 400 (1988).
[31] D. S. Bagdasaryan *et al.*, "Measurement of the spectra of (e,e') scattering ^{9}Be and ^{12}C nuclei in the inelastic region at q^2 approximately 0.4 (gev/c)^2," (1988), yERPHI-1077-40-88.
[32] M. Murphy *et al.*, Phys. Rev. C **100**, 054606 (2019), arXiv:1908.01802 [hep-ex] .
[33] J. Arrington *et al.*, Phys. Rev. **C53**, 2248 (1996), nucl-ex/9504003 .
[34] D. B. Day *et al.*, Phys. Rev. **C48**, 1849 (1993).
[35] J. Arrington *et al.*, Phys. Rev. Lett. **82**, 2056 (1999), nucl-ex/9811008 .
[36] J. Arrington *et al.*, Phys. Rev. C **104**, 065203 (2021), arXiv:2110.08399 [nucl-ex] .
[37] J. Seely *et al.*, Phys. Rev. Lett. **103**, 202301 (2009), arXiv:0904.4448 [nucl-ex] .
[38] R. R. Whitney, I. Sick, J. R. Ficenec, R. D. Kephart, and W. P. Trower, Phys. Rev. **C9**, 2230 (1974).
[39] E. J. Moniz, I. Sick, R. R. Whitney, J. R. Ficenec, R. D. Kephart, and W. P. Trower, Phys. Rev. Lett. **26**, 445 (1971).
[40] S. Alsalmi *et al.*, "Experimental investigation of the structure functions of ^{12}c in the resonance region," (2023), to be published.
[41] I. Albayrak *et al.*, "Precise measurements of electron scattering quasielastic cross sections on ^{12}c," (2023), to be published.
[42] S. A. Alsalmi, *Measurement of the Nuclear Dependence of F_2 and R=Sigma_L/Sigma_T in The Nucleon Resonance Region*, Ph.D. thesis, Kent State University, Kent State U. (2019).
[43] J. Gomez *et al.*, Phys. Rev. D **49**, 4348 (1994).
[44] "Resonance Data Archive at Jefferson Lab Hall C," Https://hallcweb.jlab.org/resdata/.
[45] N. Fomin *et al.*, Phys. Rev. Lett. **105**, 212502 (2010), arXiv:1008.2713 [nucl-ex] .
[46] Y. Liang *et al.* (Jefferson Lab Hall C E94-110), Phys. Rev. C **105**, 065205 (2022), arXiv:nucl-ex/0410027 .

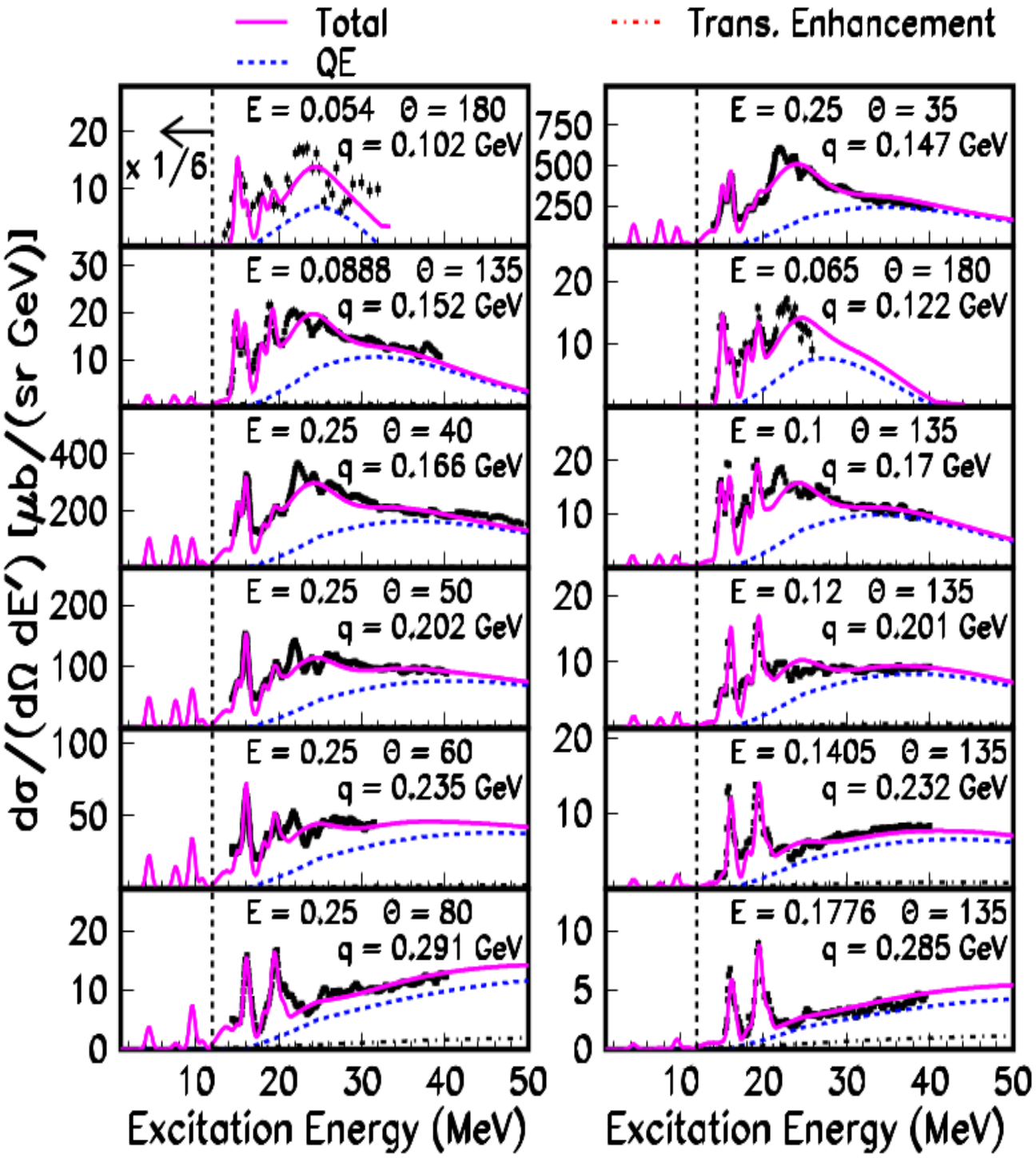

FIG. 13: Radiatively corrected inelastic electron scattering cross sections on ^{12}C for excitation energies less than 50 MeV. The cross sections for excitation energies less than 12 MeV are multiplied by (1/6). The pink solid line is the predicted total cross section from our universal fit[12, 13] to all electron scattering data on ^{12}C. The fit include nuclear excitations, a superscaling QE model[**?**] with Rosenfelder Pauli suppression[27] (dashed blue line), "Transverse Enhancement/Meson Exchange Currents" (dot-dashed line) and pion production processes (at higher excitation energies). The data are from Yamaguchi:71[6] except for the cross sections for E_o=54 MeV and 180^0 (from Goldemberg:64 [19]) and the cross sections for E_o=65 MeV and 80^0 (from Deforest:65 [20]. The measurements at 180^0 are only sensitive to the transverse form factors.

[47] W. Czyz, Phys. Rev. **131**, 2141 (1963).
[48] P. Bounin and J. R. Bishop, J. Phys, **24**, 974 (1963).
[49] J. Lovseth, Nuovo Cim. A **57**, 382 (1968).
[50] P. Antony-Spies, P. P. Delsanto, E. Spamer, A. Goldman, and O. Titze, Phys. Lett. B **31**, 632 (1970).
[51] T. W. Donnelly, J. D. Walecka, I. Sick, and E. B. Hughes, Phys. Rev. Lett. **21**, 1196 (1968).
[52] T. W. Donnelly, Nucl. Phys. A **150**, 393 (1970).
[53] D. Zeller, *Investigation of the structure of the C-12 nucleus by high-energy electron scattering (DESY-F23-73-2)*, Master's thesis, University of Karlsruhe (1973).